Inorganic Chemistry

Article

pubs.acs.org/IC

Heterolytic H−H and H−B Bond Cleavage Reactions of $\{(IPr)Ni(\mu\text{-}S)\}_2$

Frank Olechnowicz,[†] Gregory L. Hillhouse,[†,§] Thomas R. Cundari,[‡] and Richard F. Jordan*[,†]

[†]Department of Chemistry, The University of Chicago, 5735 S. Ellis Avenue, Chicago, Illinois 60637, United States

[‡]Department of Chemistry, Center for Advanced Scientific Computing and Modeling (CASCaM), University of North Texas, P.O. Box 305070, Denton, Texas 76203-5070, United States

Supporting Information

ABSTRACT: Kinetic and DFT computational studies reveal that the reaction of $\{(IPr)Ni(\mu\text{-}S)\}_2$ (**1**, IPr = 1,3-bis(2,6-diisopropyl-phenyl)-imidazolin-2-ylidene) with dihydrogen to produce $\{(IPr)Ni(\mu\text{-}SH)\}_2$ (**2**) proceeds by rate-limiting heterolytic addition of H_2 across a Ni−S bond of intact dinuclear **1**, followed by *cis/trans* isomerization at Ni and subsequent H migration from Ni to S, to produce the bis-hydrosulfide product **2**. Complex **1** reacts in a similar manner with pinacolborane to produce $\{(IPr)Ni\}_2(\mu\text{-}SH)(\mu\text{-}SBPin)$ (**3**), showing that heterolytic activation by this nickel μ-sulfide complex can be generalized to other H−E bonds.

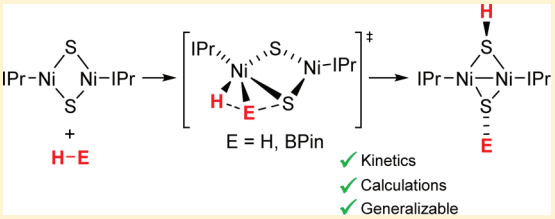

INTRODUCTION

The removal of sulfur compounds from petroleum fractions by catalytic hydrodesulfurization is an important step in the production of clean fuels.[1,2] The catalysts employed are based on MoS_2 doped with Ni or Co, and the initial activation of H_2 is a key step in these reactions. Theoretical investigations of MoS_2 catalysts have predicted that H_2 is activated heterolytically by the Mo-S-Mo units to form Mo-H and Mo-SH functionalities and that coordinatively unsaturated Mo-S-Mo sites located at the edges of the 2D lattice are more active than those at internal positions within the lattice.[3] The reactions of molecular metal sulfide complexes with H_2 have been studied to model the H_2 activation step.[4] In particular, several dinuclear $M_2(\mu\text{-}S)$ μ-sulfido complexes have been reported to react with H_2 to produce $M_2(\mu\text{-}SH)$ μ-hydrosulfide products, and experimental and computational studies have implicated several different mechanistic pathways for these processes.[5−9]

The diiridium complex $\{(Ph_3P)_2Ir(\mu\text{-}S)\}_2$ reacts with 2 equiv of H_2 to afford $\{(Ph_3P)_2IrH\}_2(\mu\text{-}S)(\mu\text{-}SH)(\mu\text{-}H)$ (Scheme 1).[5]

Scheme 1

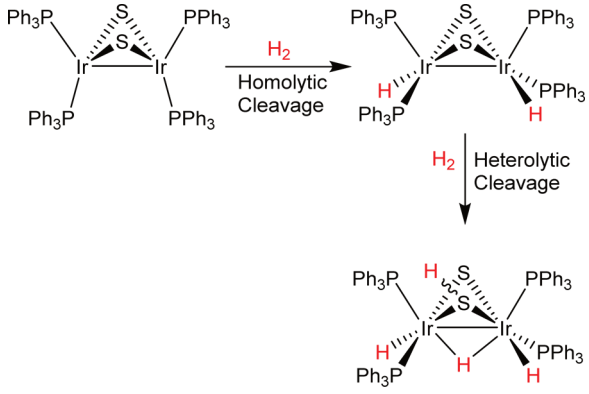

DFT computations predict that this reaction proceeds by initial oxidative addition of H_2 at one Ir center, followed by H migration to the second Ir center, which produces two terminal hydride ligands and oxidizes the Ir centers from the formal 2+ to the 3+ oxidation state. Subsequent addition of the second equiv of H_2 across the S−S vector, followed by H migration to a bridging location, produces the final product. The calculated barriers for these steps (16.8 and 16.5 kcal/mol, respectively) are consistent with the results of low-temperature NMR and isotopic labeling experiments.

$Cp_2Mo_2S_4$ complexes react with H_2 to form $Mo(\mu\text{-}SH)_2(\mu\text{-}S)_2Mo$ species (Scheme 2).[6] While the chemistry of these systems is complicated by the presence of several isomers of the reactant and product compounds,[7] a recent DFT study of the $Cp^*_2Mo_2S_4$ system proposed that the favored pathway involves concerted addition of H_2 across the two μ-S ligands to generate a $Mo(\mu\text{-}SH)_2(\mu\text{-}S_2)Mo$ intermediate, followed by cleavage of the S−S bond, to form the product.[8]

Scheme 2

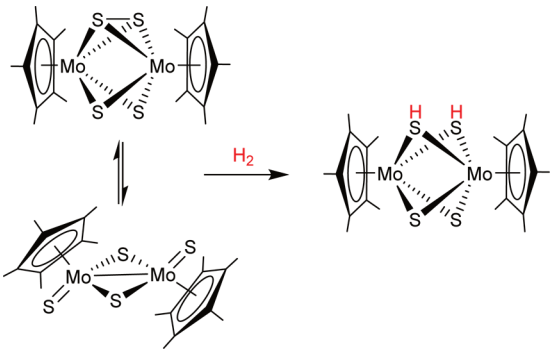

Received: June 6, 2017
Published: August 8, 2017

DOI: 10.1021/acs.inorgchem.7b01420
Inorg. Chem. 2017, 56, 9922−9930

The $\{MeC(CH_2PPh_2)_3Rh(\mu\text{-}S)\}_2^{2+}$ dication reacts reversibly with 2 equiv of H_2 at room temperature to form $\{MeC(CH_2PPh_2)_3RhH(\mu\text{-}SH)\}_2^{2+}$ (Scheme 3).[9] Low-temperature

Scheme 3

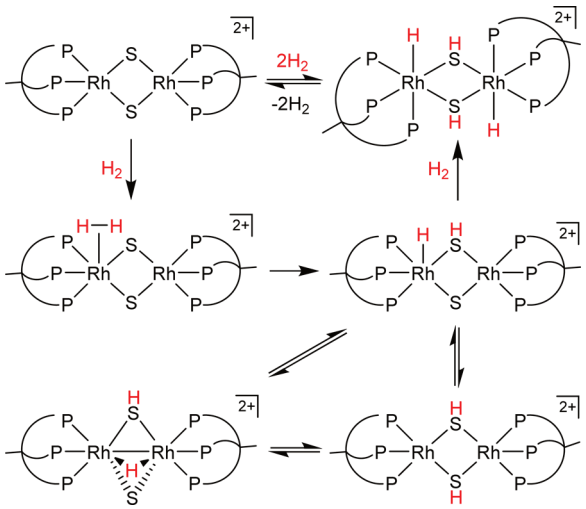

NMR studies revealed the formation of an intermediate in which all of the phosphorus atoms are equivalent on the NMR time scale at −80 °C. DFT calculations predict that this reaction proceeds by two sequential heterolytic H_2 additions across the Rh−S bonds with barriers of 7.2 and 8.0 kcal/mol. The calculations also predict that, in addition to the Rh(μ-H)(μ-SH)Rh intermediate, Rh(μ-SH)$_2$Rh and Rh(μ-H)(μ-SH)(μ-S)Rh species are energetically accessible.

We recently reported that $\{(IPr)Ni(\mu\text{-}S)\}_2$ (**1**, IPr = 1,3-bis(2,6-diisopropyl-phenyl)imidazolin-2-ylidene) reacts cleanly with H_2 to produce $\{(IPr)Ni(\mu\text{-}SH)\}_2$ (**2**, Scheme 4).[10] This

Scheme 4

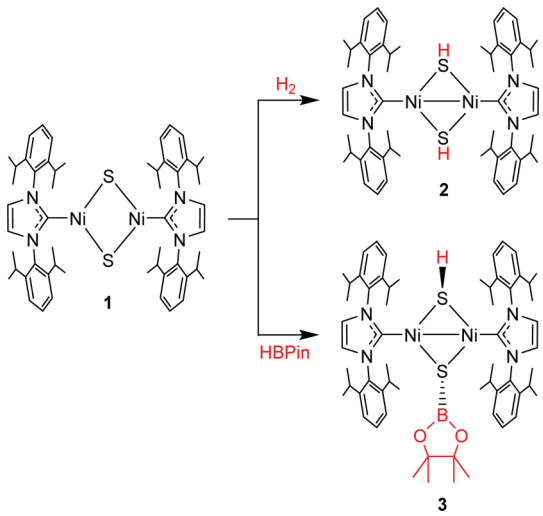

system provides a simple and well-behaved reaction to study the activation of H_2 and develop an improved understanding of how $M_2(\mu\text{-}S)_2$ complexes react with this substrate. Here we describe kinetic and DFT computational studies that show that this process occurs by rate-limiting heterolytic addition of H_2 across a Ni−S bond of the intact dimer **1**, followed by *cis*/*trans* isomerization at Ni and subsequent H migration from Ni to S, to form **2**. We also report that **1** reacts with HBPin (Pin = 2,3-dimethylbutane-2,3-diolate) in a similar manner, showing that this heterolytic activation pathway can be generalized to other E−H bonds.

RESULTS AND DISCUSSION

Kinetics of the Reaction of 1 and H_2. Kinetic studies of the reaction of **1** with H_2 were performed to establish if the intact dimer reacts directly with H_2 or must first dissociate into monomeric fragments, and if the H_2 activation is the rate-determining step. The kinetics were measured by ^{1}H NMR spectroscopy by monitoring the imidazole resonances of starting material **1** and product **2**, which are sharp and well-separated from other resonances, using C_6Me_6 as an internal standard. A representative set of spectra is shown in Figure 1. The only observed species were **1**, **2**, and thermal decomposition products from **2**.[11] No intermediates were observed.

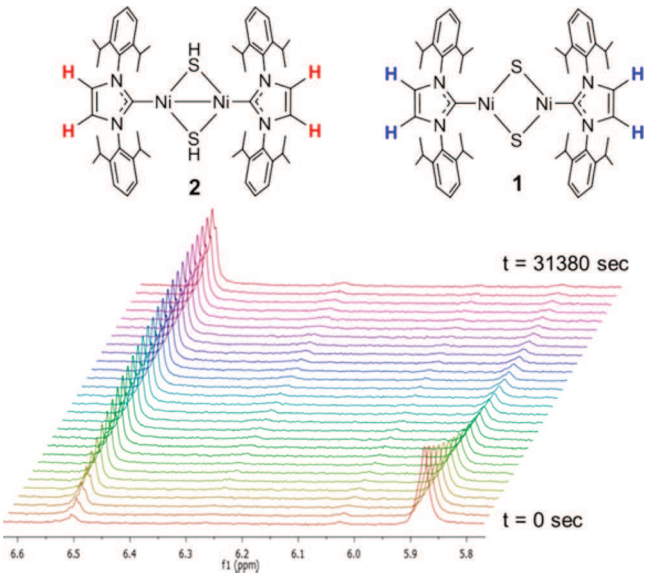

Figure 1. ^{1}H NMR monitoring of the reaction of **1** with H_2 to produce **2**. The imidazole region of the spectrum is shown. Concentration versus time data corresponding to these spectra are given in Figure 2. Conditions: benzene solvent, 80 °C, 5 atm H_2, $[\mathbf{1}]_0$ = 0.0037 M.

As shown in Figure 2, these kinetic data fit the first-order rate law in eq 1. As ESI-MS results establish that the dimeric structure of **1** is maintained in solution (see the Supporting Information), this rate law implies that dinuclear **1** remains intact in the rate-limiting step.

$$\text{Rate} = -d[\mathbf{1}]/dt = k_{obs}[\mathbf{1}] \quad (1)$$

Kinetic runs at different H_2 pressures were performed to determine the reaction order in H_2 (Figure 3). The rate increases linearly with increasing H_2 pressure, indicating that the reaction is first-order in H_2.[12] The full rate law is given in eq 2

$$\text{Rate} = -d[\mathbf{1}]/dt = k[\mathbf{1}]P_{H_2} \quad (2)$$

where $k = 5.7(1) \times 10^{-3}$ s^{-1} atm^{-1} at 80 °C.

The kinetic isotope effect (KIE) was determined to be k_H/k_D = 1.8(1) by comparing the rates of the reaction of **1** with 1 atm of H_2 or D_2 in J. Young NMR tubes at 80 °C. The μ-*SH*

DOI: 10.1021/acs.inorgchem.7b01420
Inorg. Chem. 2017, 56, 9922−9930

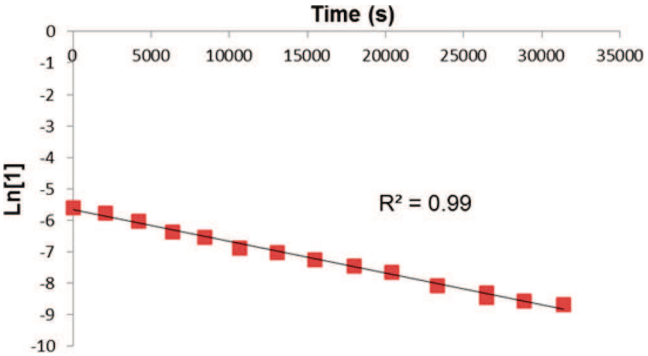

Figure 2. Plot of ln[**1**] versus time for the reaction of **1** with H_2 to form **2** from Figure 1. Conditions: benzene solvent, 80 °C, 5 atm H_2, $[\mathbf{1}]_0$ = 0.0037 M.

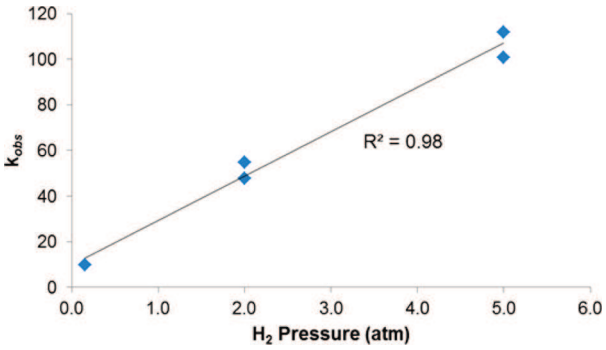

Figure 3. Plot of the observed rate constant k_{obs} versus H_2 pressure for the reaction of **1** with H_2. Conditions: benzene solvent, 80 °C and $[\mathbf{1}]_0 \approx 0.0037$ M.

resonance of **2** was not observed in the D_2 reaction, confirming that deuterium is incorporated at this site as expected. Additionally, control experiments establish that no deuterium scrambling between **2** and D_2 occurs under the reaction conditions. This KIE value is characteristic of a primary isotope effect and provides evidence that H−H bond cleavage occurs during the rate-limiting step of this reaction. While KIE values are not available for the reactions in Schemes 1−3, a KIE of 2.0(1) was measured for H_2 addition to a mononuclear Ru-amide complex,[13] and KIEs of 1.8−2.4 were reported for the addition of H_2 to dinuclear Zr-N_2 complexes.[14]

DFT Computational Investigation. DFT calculations were undertaken to elucidate the reaction pathway for the hydrogenation of **1**. The B3PW91 functional was used as it performed well in model geometry optimizations and was reasonably time-efficient for these systems (see the Supporting Information).

The calculated free energy surface for the hydrogenation of **1** is shown in Figure 4. The starting point for the reaction is the open shell singlet (OSS) structure of **1** and H_2. The first and rate-limiting step is heterolytic addition of H_2 across the Ni−S bond within the Ni_2S_2 plane, which has a free energy barrier of 30.9 kcal/mol and produces a *cis*-hydride μ-hydrosulfide species (*cis*-(H)(SH)) as a local minimum at 6.0 kcal/mol relative to separated reactants. In the *cis* conformation, the H atom cannot migrate to the remaining bridging sulfide (to which it is *trans*), so the complex must isomerize. The *cis*/*trans* isomerization occurs via a pseudo-tetrahedral transition state with a barrier of 14.7 kcal/mol and produces the *trans*-hydride-hydrosulfide species (*trans*-(H)(SH)) at a relative free energy of 6.6 kcal/mol. The Ni-*H* atom then migrates to the bridging sulfide to form the product {(IPr)Ni(μ-SH)}$_2$ (**2**). There are two isomers of **2** with *syn* and *anti* configurations of the μ-SH ligands at −3.0 and −4.0 kcal/mol, respectively, and transition states leading to both configurations were found at 27.4 and 22.2 kcal/mol, respectively. The KIE calculated by substituting D_2 in place of H_2 for relevant structures is 1.9, which agrees well with the experimental value of 1.8(1). Overall, the reaction is close to thermoneutral (ΔG = −4 kcal/mol). The computed barrier of 30.9 kcal/mol agrees well with that calculated from the experimental k_{obs} value determined at 80 °C and 1 atm H_2 by the Eyring equation (29.1(3) kcal/mol). Other H_2 activation mechanisms were investigated (see the Supporting Information), but the calculated barriers were much higher than that in Figure 4. A key factor that favors the mechanism in Figure 4 over other pathways is that, during the rate-limiting H_2 activation step, a simple pivoting of the IPr ligand around the Ni_2S_2 plane is sufficient to accommodate the H_2 molecule without steric clashing of the aryl rings of the two IPr ligands.

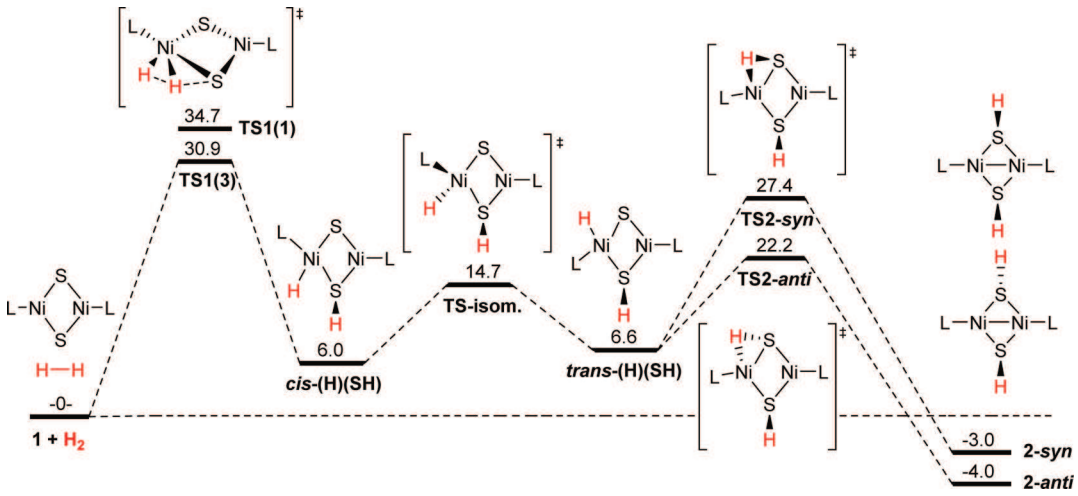

Figure 4. Calculated reaction pathway for the hydrogenation of **1**. All structures were optimized with B3PW91/6-31+G(d) as functional and basis set. Energies are ΔG-corrected and reported in kcal/mol, with the starting materials defined as 0. All species are singlets, except for the first transition state, for which singlet (TS1(1)) and triplet (TS1(3)) states were found at similar energies. L = 1,3-bis(2,6-diisopropyl-phenyl)imidazolin-2-ylidene.

DOI: 10.1021/acs.inorgchem.7b01420
Inorg. Chem. 2017, 56, 9922−9930

In contrast, other possible pathways (e.g., heterolytic addition of H_2 from above the Ni_2S_2 plane and addition of H_2 across the Ni−Ni vector) require displacement of the IPr ligands out of the Ni_2S_2 plane and result in significant steric clashing. The H_2 activation step converts one Ni-S-Ni unit to a Ni(H)(μ-SH)Ni unit and does not change the oxidation state at Ni (both Ni centers remain Ni^{II}). The movement of the Ni-*H* atom from Ni to the remaining S^{2-} ligand may be viewed as a reductive elimination that reduces one Ni^{II} to Ni^0. Accompanying electronic rearrangement produces two Ni^I centers.

Reaction of 1 with Pinacolborane. The conclusion that the hydrogenation of **1** proceeds by heterolytic addition of H_2 across a Ni−S bond suggests that other substrates that undergo heterolytic bond activation may display similar reactivity. The B−H bonds of boranes are often activated in a heterolytic manner.[15] The reaction of the **1** with HBPin (Pin = 2,3-dimethylbutane-2,3-diolate) in Et_2O produces {(IPr)Ni}$_2$(μ-SH)(μ-SBPin) (**3**) within seconds at room temperature (Scheme 4). The reaction is quantitative as measured by ^{1}H NMR and is accompanied by a color change from turquoise to yellow.

The solid-state structure of **3** was determined by X-ray diffraction (Figure 5). Compound **3** assumes a bimetallic structure with planar Ni centers (sum of angles: 359.2(2)°, 359.2(2)°) linked by μ-SH and μ-SBPin ligands that are arranged in an *anti* configuration. The hydrosulfide hydrogen atom was located in the difference map, and its position was refined isotropically. The Ni_2S_2 core adopts a diamond shape with acute angles at S and obtuse angles at Ni. The Ni−Ni distance (2.4302(5) Å) is slightly longer than that in **2** (2.3601(7) Å) but still well within the range observed for Ni(I)-Ni(I) species with antiferromagnetically coupled Ni centers (2.314(1)−2.559(2) Å).[16] The imidazolin-2-ylidene rings are oriented nearly perpendicular to the corresponding NiS_2 planes (72.3° and 85.9°). The μ-SH group is sandwiched by two diisopropyl-phenyl rings. The boron center adopts the expected trigonal planar geometry (sum of angles: 360.0(7)°), and the S−B distance (1.804(3) Å) is in the normal range for B−S bonds in 3-coordinate B compounds.[17]

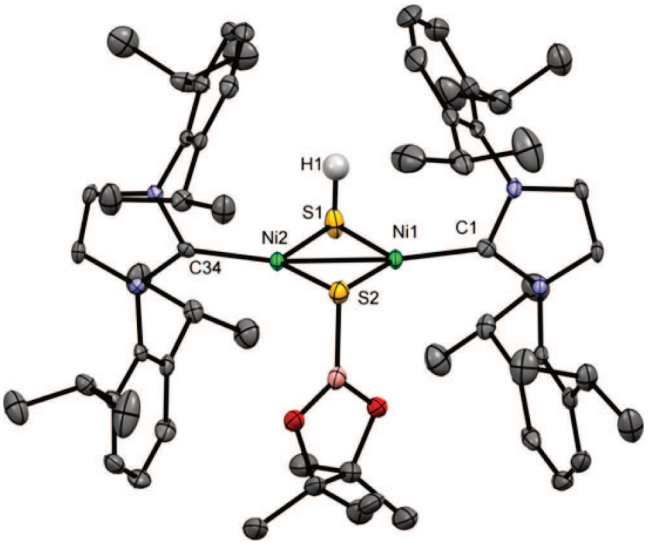

Figure 5. Molecular structure of {(IPr)Ni}$_2$(μ-SH)(μ-SBPin) (**3**). Hydrogen atoms except for the S-H hydrogen are omitted. Selected bond distances (Å) and angles (deg): Ni(1)−Ni(2) = 2.4302(5), Ni(1)−S(1) = 2.1945(8), Ni(1)−S(2) = 2.2220(8), Ni(2)−S(1) = 2.2089(8), Ni(2)−S(2) = 2.2260(8), Ni(1)−C(1) = 1.889(2), Ni(2)−C(34) = 1.892(2), S(2)−B(1) = 1.804(3); Ni(1)−S(1)−Ni(2) = 66.99(2), Ni(1)−S(2)−Ni(2) = 66.24(2), S(1)−Ni(1)−S(2) = 113.67(3), S(1)−Ni(2)−S(2) = 112.94(3), C(1)−Ni(1)−S(1) = 121.16(8), C(1)−Ni(1)−S(2) = 124.35(8), C(34)−Ni(2)−S(1) = 115.51(8), C(34)−Ni(2)−S(2) = 130.74(8).

The ^{1}H NMR spectrum of **3** in benzene-d_6 solution at room temperature contains a μ-SH resonance (1H) at δ = −6.1, which is ca. 1.3 ppm upfield compared to that of **2** (δ = −4.8) and is consistent with the anisotropic shielding by the two diisopropyl-phenyl rings expected from the solid-state structure. The spectrum also contains two methyl resonances and one methine resonance, indicating that all four isopropyl groups are equivalent on the NMR time scale. At 215 K, the ^{1}H NMR resonances of **3** are broadened but not split. Rotation around the Ni−carbene bond is probably fast, based on results for **2**, but this process does not permute all four isopropyl groups.[10] Rotation around the Ni−carbene bond combined with rotation around the N−aryl bonds would permute the four isopropyl groups, but based on results for other systems, the barrier to the latter process is probably too high for it to be operable at 215 K.[18] However, stereochemical inversion at the S centers combined with Ni−carbene bond rotation will exchange all four isopropyl groups. Low sulfur inversion barriers have been reported for the μ-SR complexes {(dippe)Rh(μ-SPh)}$_2$ (7.7 kcal/mol) and {(dippe)Rh(μ-S(*o*-biphenyl))}$_2$ (14.7 kcal/mol),[19] while a much higher barrier was reported for the terminal-SR complex {(Cp)(CO)Fe(μ-SPh)}$_2$ (30.7 kcal/mol).[20] Sulfur inversion barriers as low as 11.2 kcal/mol have been measured for Ru, Pd, and Pt thioether complexes.[21]

The ^{11}B NMR resonance of **3** appears at δ = 25.2, slightly upfield from those of {Rh(PEt$_3$)$_2$(SBPin)}$_2$(μ-C) (δ 33.6),[22] Os(P^{i}Pr$_3$)$_2$(H)(H$_2$)(SBPin) (δ 35),[23] and organic borylthiolates (δ 32.8−33.7).[24,25]

Complex **3** is an unusual example of a crystallographically characterized compound that contains a borylthiolate ligand.[26] The terminal −SBPin complex {Rh(PEt$_3$)$_2$(SBPin)}$_2$(μ-C) was formed by the reaction of CS_2 with Rh(PEt$_3$)$_3$(BPin), which proceeds with complete C−S bond cleavage to generate the borylthiolate ligand.[22] The Os(II) complex Os(P^{i}Pr$_3$)$_2$(H)(H$_2$)(SBPin) was synthesized by the reaction of Os(P^{i}Pr$_3$)$_2$(H)(SH) and HBPin, which proceeds by addition of the H−B bond across the Os−S bond and subsequent H migration from S to Os.[23] Several mononuclear metal thiolate and sulfide complexes have been reported to undergo E−H bond activation reactions similar to those observed for **1**.[27]

■ CONCLUSIONS

Kinetic and computational studies reveal that {(IPr)Ni(μ-S)}$_2$ (**1**) reacts with H_2 to produce {(IPr)Ni(μ-SH)}$_2$ (**2**) via rate-limiting heterolytic addition of H_2 across a Ni−S bond of intact **1**, followed by cis/trans isomerization at Ni and subsequent H migration from Ni to S. This pathway is analogous to that implicated for the {MeC(CH$_2$PPh$_2$)$_3$Rh(μ-S)}$_2^{2+}$ system.[9] Complex **1** reacts similarly with pinacolborane to produce {(IPr)Ni}$_2$(μ-SH)(μ-SBPin) (**3**), showing that this reaction can be generalized to other H−E bonds.

■ EXPERIMENTAL SECTION

General Procedures. All experiments were performed under nitrogen using drybox or Schlenk techniques. Nitrogen was purified by passage through activated molecular sieves and a Q-5 oxygen

DOI: 10.1021/acs.inorgchem.7b01420
Inorg. Chem. 2017, 56, 9922−9930

Table 1. Crystal Data and Structure Refinement for $(IPrNi)_2(\mu\text{-SH})(\mu\text{-SBPin})$ (3)

empirical formula	$C_{62}H_{90}BN_4Ni_2O_{2.5}S_2$
formula weight	1123.72
temperature/K	100(2)
crystal system	monoclinic
space group	$P2_1/c$
a/Å	25.528(3)
b/Å	12.3656(13)
c/Å	20.065(2)
α/deg	90
β/deg	103.772(3)
γ/deg	90
volume/Å^3	6152.1(11)
Z	4
ρ_{calc}/g/cm^3	1.213
μ/mm^{-1}	0.724
F(000)	2412.0
crystal size/mm^3	0.08 × 0.06 × 0.02
radiation	MoKα (λ = 0.71073)
2Θ range for data collection/deg	4.662−51.506
index ranges	$-31 \le h \le 31$, $-15 \le k \le 15$, $-24 \le l \le 22$
reflns collected	82 382
independent reflns	11 404 [R_{int} = 0.0742, R_{sigma} = 0.0724]
data/restraints/parameters	11 404/481/787
goodness-of-fit on F^2	1.007
final R indexes [$I \ge 2\sigma(I)$]	R_1 = 0.0441, wR_2 = 0.0760
final R indexes [all data]	R_1 = 0.0910, wR_2 = 0.0876
largest diff. peak/hole/e Å^{-3}	0.44/−0.48

scavenger. Anhydrous Et_2O and THF were purified by passage through activated alumina.[28] Anhydrous benzene, pentane, and toluene were purified by passage through activated alumina and a BASF R3-11 oxygen scavenger. C_6D_6 was purchased from Cambridge Isotope Laboratories, degassed by freeze−pump−thaw cycles, and dried over Na-benzophenone ketyl or activated Linde 4 Å molecular sieves. Celite and 4 Å molecular sieves were activated by evacuation overnight at 180 °C. Pinacolborane was purchased from Sigma-Aldrich and used as received. $\{(IPr)Ni(\mu\text{-S})\}_2$ was prepared as described previously.[10] All other chemicals were used as received. ^1H and ^{13}C NMR spectra were recorded on a Bruker DRX-500 spectrometer at room temperature using Teflon-valved tubes. ^1H and ^{13}C NMR chemical shifts are reported relative to $SiMe_4$ and were determined by reference to the residual solvent resonances (^1H: residual C_6D_5H in C_6D_6 δ 7.16; ^{13}C: C_6D_6 δ 128.1). Coupling constants are given in hertz (Hz). ^{11}B NMR spectra were collected on a Bruker DRX-400 spectrometer and are reported relative to externally referenced $BF_3\cdot Et_2O$ (δ = 0). Mass spectrometry was performed on Agilent 6224 TOF-MS (high resolution) or 6130 LCMS (low resolution) instruments.

*{(IPr)Ni}$_2$(μ-SH)(μ-SBPin) (**3**).* Neat HBPin (5.5 μL, 0.038 mmol) was added dropwise via microsyringe to a solution of **1** (0.0360 g, 0.038 mmol) in Et_2O (5 mL) while the mixture was stirred. The color turned from turquoise to bright green to neon yellow within 10 s. The solution was stirred for 5 min and transferred to a scintillation vial. The solution was chilled to −35 °C overnight, and the resulting yellow crystals were collected by vacuum filtration. Yield: 0.0187 g (46%). X-ray quality crystals were grown by liquid diffusion of pentane into an Et_2O solution of **3** at −35 °C. ^1H NMR (C_6D_6): δ 7.35 (t, J = 7.5, 4H), 7.25 (d, J = 7.5, 8H), 6.45 (s, 4H), 3.05 (sept, J = 6.5, 8H), 1.53 (d, J = 6.5, 24H), 1.11 (d, J = 6.5, 24H), 0.89 (s, 12H), −6.09 (s, 1H). $^{13}C\{^1H\}$ NMR (C_6D_6): δ 187.2 (Ni-CN_2), 146.9 (o-$C_6{}^iPr_2H_3$), 138.0 (i-$C_6{}^iPr_2H_3$), 129.4 (p-$C_6{}^iPr_2H_3$), 124.4 ($CN_2C_2H_2$), 124.2 (m-$C_6{}^iPr_2H_3$), 82.1 ($BO_2C_2Me_4$), 28.9 (Ar-$CHMe_2$), 25.1 ($ArCH(CH_3)_2$), 25.0 ($ArCH(CH_3)_2$), 24.4 ($BO_2C_2(CH_3)_4$). $^{11}B\{^1H\}$ NMR (C_6D_6): δ 25.2.

*X-ray Data Collection and Structure Refinement for **3**.* A yellow plate of **3** was mounted on a Dual-Thickness MicroMount (MiTeGen) with a 30 μm sample aperture with Fluorolube oil. Diffraction data were collected at 100 K on a Bruker D8 VENTURE diffractometer equipped with a microfocus Mo-target X-ray tube (λ = 0.71073 Å) and PHOTON 100 CMOS detector. Data reduction and integration were performed with the Bruker APEX3 software package (Bruker AXS, version 2015.5-2, 2015). The data were scaled and corrected for absorption effects using the multiscan procedure as implemented in SADABS (Bruker AXS, version 2014/5, 2015, part of Bruker APEX3 software package). The structure was solved by SHELXT (Version 2014/5)[29] and refined by a full-matrix least-squares procedure using OLEX2[30] (XL refinement program version 2014/7).[31] Crystallographic data and details of the data collection and structure refinement are listed in Table 1.

All atoms were refined with anisotropic thermal parameters. Hydrogen atoms were included in idealized positions for structure factor calculations except the H atom attached to S1, which was found in the difference Fourier map and refined without any geometric restraints. Its thermal parameter was constrained to be 1.2 times that of the S1 atom. The pinacolate group was found to be disordered over two rotational orientations (refined to an 82/18 occupancies ratio). This disorder was modeled with the application of geometric (SADI) restraints and using enhanced rigid body restraints (RIGU) for the thermal parameters. A solvent molecule was located on the edge of two unit cells and was modeled as Et_2O. All structures are drawn with thermal ellipsoids at 50% probability.

Kinetic Studies. Kinetic runs at 1 atm of H_2 or D_2 were performed in J. Young NMR tubes. Compound **1** and the internal standard C_6Me_6 were loaded into the tube inside a glovebox. C_6D_6 was vacuum-transferred into the tube from a Na-benzophenone ketyl solution, and the tube was pressurized with H_2 or D_2. The tube was heated to 80 °C, and NMR spectra were taken periodically until the reaction had proceeded for five half-lives.

Reactions at 0.2, 2, and 5 atm H_2 were performed in a Fischer-Porter bottle. Compound **1** and the internal standard C_6Me_6 were dissolved in C_6D_6, and loaded into the bottle along with a stir bar

DOI: 10.1021/acs.inorgchem.7b01420
Inorg. Chem. 2017, 56, 9922−9930

inside a glovebox. The bottle was removed from the glovebox and attached to a Schlenk line and a H_2 cylinder. The headspace was saturated with H_2 by 10 cycles of charging with H_2 and discharging by vacuum. The apparatus was then pressurized to the desired pressure of H_2 and heated to 80 °C, which was denoted as the start of the reaction. The reaction mixture was sampled periodically for 12 h or until the reaction had proceeded for five half-lives. The sampling was performed by reducing the pressure, withdrawing 0.6 mL of the mixture by syringe, and transferring it to a nitrogen-flushed NMR tube for ^{1}H NMR analysis. The Fischer-Porter bottle was repressurized with H_2 and the reaction resumed. This entire sampling process was typically completed within 3 min, a negligible amount of time for a reaction that takes more than 8 h to go to completion. The sample was cooled to room temperature and a ^{1}H NMR spectrum was collected.

DFT Calculations. Density functional theory calculations were performed with the Gaussian 09 package.[32] The reaction coordinate for the full IPr ligand was explored at the ONIOM[33] (B3PW91/6-31+G(d):UFF)[34] level of theory. The 2,6-diisopropyl-phenyl rings were included in the UFF partition, and the remainder of the complex modeled with B3PW91/6-31+G(d). Unless otherwise noted, calculations were for the gas phase and assumed 298.15 K and 1 atm. All calculated free energies are reported in kcal/mol. Optimized ground states contained no imaginary vibrational frequencies, and optimized transition states contained one imaginary vibrational frequency.

■ ASSOCIATED CONTENT

Supporting Information

The Supporting Information is available free of charge on the ACS Publications website at DOI: 10.1021/acs.inorgchem.7b01420.

Characterization of **3**, kinetic investigation of the reaction of **1** with H_2, computational investigation, references, and calculated atomic coordinates (PDF)

Crystallographic experimental section (PDF)

Accession Codes

CCDC 1555657 contains the supplementary crystallographic data for this paper. These data can be obtained free of charge via www.ccdc.cam.ac.uk/data_request/cif, or by emailing data_request@ccdc.cam.ac.uk, or by contacting The Cambridge Crystallographic Data Centre, 12 Union Road, Cambridge CB2 1EZ, UK; fax: +44 1223 336033.

■ AUTHOR INFORMATION

Corresponding Author

*E-mail: rfjordan@uchicago.edu.

ORCID

Richard F. Jordan: 0000-0002-3158-4745

Notes

The authors declare no competing financial interest.

[§]Deceased March 6, 2014.

■ ACKNOWLEDGMENTS

The research at The University of Chicago was supported by the National Science Foundation through grants CHE-1266281, CHE 1709159, and CHE-1048528 (CRIF MU instrumentation) and the Department of Education through grant P200A120093. The research at the University of North Texas was supported by the U.S. Department of Energy, Office of Basic Energy Sciences (Chemical Sciences, Geosciences and Biosciences Division), via grant number DE-FG02-03ER15387. The authors acknowledge the National Science Foundation for their support of the UNT Chemistry CASCaM high performance computing facility through grant CHE-1531468. We thank Alex Filatov for assistance with X-ray crystallography.

■ REFERENCES

(1) (a) Clausen, B. S.; Topsoe, H.; Massoth, F. E. *Hydrotreating Catalysis*; Anderson, J., Boudart, M., Eds.; Springer: Berlin, 1996; Vol. *11*. (b) Sanchez-Delgado, R. A. *Organometallic Modeling of the Hydrodesulfurization and Hydrodenitrogenation Reactions*; Kluwer Academic Publishers: Dordrecht, 2002. (c) Stanislaus, A.; Marafi, A.; Rana, M. S. Recent advances in the science and technology of ultra low sulfur diesel (ULSD) Production. *Catal. Today* **2010**, *153*, 1−68. (d) Song, C. An overview of new approaches to deep desulfurization forultra-clean gasoline, diesel fuel and jet fuel. *Catal. Today* **2003**, *86*, 211−263. (e) Breysse, M.; Furimsky, E.; Kasztelan, S.; Lacroix, M.; Perot, G. Hydrogen Activation by Transition Metal Sulfides. *Catal. Rev.: Sci. Eng.* **2002**, *44*, 651.

(2) (a) Hein, J.; Gutiérrez, O. Y.; Albersberger, S.; Han, J.; Jentys, A.; Lercher, J. A. Towards Understanding Structure−Activity Relationships of Ni−Mo−W Sulfide Hydrotreating Catalysts. *ChemCatChem* **2017**, *9*, 629. (b) Han, W.; Nie, H.; Long, X.; Lí, M.; Yang, Q.; Li, D. Effects of the support Brønsted acidity on the hydrodesulfurization and hydrodenitrogention activity of sulfided NiMo/Al_2O_3 catalysts. *Catal. Today* **2017**, *292*, 58. (c) Schachtl, E.; Yoo, J. S.; Gutiérrez, O. Y.; Studt, F.; Lercher, J. A. Impact of Ni promotion on the hydrogenation pathways of phenanthrene on MoS_2/γ-Al_2O_3. *J. Catal.* **2017**, *352*, 171. (d) Albersberger, S.; Hein, J.; Schreiber, M. W.; Guerra, S.; Han, J.; Gutiérrez, O. Y.; Lercher, J. A. Simultaneous hydrodenitrogenation and hydrodesulfurization on unsupported Ni-Mo-W sulfides. *Catal. Today* **2017**. (e) Ferraz, S. G. A.; Santos, B. M.; Zotin, F. M. Z.; Araujo, L. R. R.; Zotin, J. L. Influence of Support Acidity of NiMo Sulfide Catalysts for Hydrogenation and Hydrocracking of Tetralin and Its Reaction Intermediates. *Ind. Eng. Chem. Res.* **2015**, *54*, 2646. (f) Gutiérrez, O.; Singh, S.; Schachtl, E.; Kim, J.; Kondratieva, E.; Hein, J.; Lercher, J. A. Effects of the Support on the Performance and Promotion of (Ni)MoS_2 Catalysts for Simultaneous Hydrodenitrogenation and Hydrodesulfurization. *ACS Catal.* **2014**, *4*, 1487. (g) Lai, W.; Chen, Z.; Zhu, J.; Yang, L.; Zheng, J.; Yi, X.; Fang, W. A NiMoS flower-like structure with self-assembled nanosheets as high-performance hydrodesulfurization catalysts. *Nanoscale* **2016**, *8*, 3823. (h) Scott, C. E.; Perez-Zurita, M. J.; Carbognani, L. A.; Molero, H.; Vitale, G.; Guzman, H. J.; Pereira-Almao, P. Preparation of NiMoS nanoparticles for hydrotreating. *Catal. Today* **2015**, *250*, 21. (i) Torres-Nieto, J.; Brennessel, W. W.; Jones, W. D.; Garcia, J. J. Mechanistic Insights on the Hydrodesulfurization of Biphenyl-2-thiol with Nickel Compounds. *J. Am. Chem. Soc.* **2009**, *131*, 4120. (j) Vicic, D. A.; Jones, W. D. Evidence for the Existence of a Late-Metal Terminal Sulfido Complex. *J. Am. Chem. Soc.* **1999**, *121*, 4070. (k) Vicic, D. A.; Jones, W. D. Modeling the Hydrodesulfurization Reaction at Nickel. Unusual Reactivity of Dibenzothiophenes Relative to Thiophene and Benzothiophene. *J. Am. Chem. Soc.* **1999**, *121*, 7606.

(3) (a) Rangarajan, S.; Mavrikakis, M. On the Preferred Active Sites of Promoted MoS_2 for Hydrodesulfurization with Minimal Organonitrogen Inhibition. *ACS Catal.* **2017**, *7*, 501. (b) Lazar, P.; Otyepka, M. Role of the Edge Properties in the Hydrogen Evolution Reaction on MoS_2. *Chem. - Eur. J.* **2017**, *23*, 4863. (c) Dugulan, A. I.; van Veen, J. A. R.; Hensen, E. J. M. On the structure and hydrotreating performance of carbon-supported CoMo- and NiMo-sulfides. *Appl. Catal., B* **2013**, *142−143*, 178. (d) Wen, X. D.; Zeng, T.; Teng, B. T.; Zhang, F.-Q.; Li, Y. W.; Wang, J.; Jiao, H. Hydrogen adsorption on a $Mo_{27}S_{54}$ cluster: A density functional theory study. *J. Mol. Catal. A: Chem.* **2006**, *249*, 191. (e) Cristol, S.; Paul, J. F.; Payen, E.; Bougeard, D.; Clémendot, S.; Hutschka, F. Theoretical Study of the MoS_2 (100) Surface: A Chemical Potential Analysis of Sulfur and Hydrogen Coverage. 2. Effect of the Total Pressure on Surface Stability. *J. Phys. Chem. B* **2002**, *106*, 5659. (f) Alexiev, V.; Prins, R.; Weber, T. DFT study of MoS_2 and hydrogen adsorbed on the $(10\bar{1}0)$ face of MoS_2. *Phys. Chem. Chem. Phys.* **2001**, *3*, 5326. (g) Cristol, S.; Paul, J. F.; Payen, E.; Bougeard, D.; Clémendot, S.; Hutschka, F. Theoretical Study of the MoS_2 (100) Surface: A Chemical Potential Analysis of Sulfur and Hydrogen Coverage. *J. Phys. Chem. B* **2000**, *104*, 11220. (h) Neurock, M.; van Santen, R. A. Theory of Carbon-Sulfur Bond

DOI: 10.1021/acs.inorgchem.7b01420
Inorg. Chem. 2017, 56, 9922−9930

Activation by Small Metal Sulfide Particles. *J. Am. Chem. Soc.* **1994**, *116*, 4427.

(4) (a) Matsumoto, T.; Nakaya, Y.; Tatsumi, K. Heterolytic dihydrogen activation by a sulfido- and oxo-bridged dinuclear germanium-ruthenium complex. *Angew. Chem., Int. Ed.* **2008**, *47*, 1913−1915. (b) Ohki, Y.; Matsuura, N.; Marumoto, T.; Kawaguchi, H.; Tatsumi, K. Heterolytic Cleavage of Dihydrogen Promoted by Sulfido-Bridged Tungsten-Ruthenium Dinuclear Complexes. *J. Am. Chem. Soc.* **2003**, *125*, 7978−7988. (c) Kato, H.; Seino, H.; Mizobe, Y.; Hidai, M. Syntheses and reactivities of hydrosulfido- or sulfido-bridged heterobimetallic complexes containing Group 6 and Group 9 metals. *J. Chem. Soc., Dalton Trans.* **2002**, 1494. (d) Hobert, S. E.; Noll, B. C.; Rakowski DuBois, M. Synthesis of a Rhenium(V) Polysulfide Complex and a Study of Its Reactivity with Hydrogen. *Organometallics* **2001**, *20*, 1370−1375. (e) Sweeney, Z. K.; Polse, J. L.; Bergman, R. G.; Andersen, R. A. Dihydrogen Activation by Titanium Sulfide Complexes. *Organometallics* **1999**, *18*, 5502−5510. (f) Sweeney, Z. K.; Polse, J. L.; Andersen, R. A.; Bergman, R. G.; Kubinec, M. G. Synthesis, Structure, and Reactivity of Monomeric Titanocene Sulfido and Disulfide Complexes. Reaction of H_2 with a Terminal M = S Bond. *J. Am. Chem. Soc.* **1997**, *119*, 4543−4544.

(5) (a) Algarra, A. G. Computational Insights on the Mechanism of H_2 Activation at $Ir_2S_2(PPh_3)_4$: A Combination of Multiple Reaction Pathways Involving Facile H Migration Processes. *Inorg. Chem.* **2017**, *56*, 186. (b) Rauchfuss, T. B. Research on Soluble Metal Sulfides: From Polysulfido Complexes to Functional Models for the Hydrogenases. *Inorg. Chem.* **2004**, *43*, 14. (c) Linck, R. C.; Pafford, R. J.; Rauchfuss, T. B. Heterolytic and Homolytic Activation of Dihydrogen at an Unusual Iridium (II) Sulfide. *J. Am. Chem. Soc.* **2001**, *123*, 8856. (d) Mueting, A. M.; Boyle, P. D.; Wagner, R.; Pignolet, L. H. Reaction of H_2S with $[Ir(H)_2(Me_2CO)_2(PPh_3)_2]BF_4$. Crystal and molecular structures of $[Ir_2(SH)_2(H)_3(PPh_3)_4]BF_4\cdot 2(CH_3)_2CO$, $[Ir_2S(SH)(H)_3(PPh_3)_4]\cdot 1.5C_6H_6$, and $[Ir_2(SH)(SC_3H_7)(H)_3(PPh_3)_4]BF_4\cdot(CH_3)_2CO$ and their reactions with organic reagents. *Inorg. Chem.* **1988**, *27*, 271.

(6) (a) Appel, A. M.; Lee, S.-J.; Franz, J. A.; DuBois, D. L.; DuBois, M. R. Free Energy Landscapes for S−H Bonds in $Cp^*_2Mo_2S_4$ Complexes. *J. Am. Chem. Soc.* **2009**, *131*, 5224. (b) Appel, A. M.; Lee, S.-J.; Franz, J. A.; DuBois, D. L.; Rakowski DuBois, M.; Twamley, B. Determination of S−H Bond Strengths in Dimolybdenum Tetrasulfide Complexes. *Organometallics* **2009**, *28*, 749. (c) Casewit, C. J.; Coons, D. E.; Wright, L. L.; Miller, W. K.; Rakowski DuBois, M. Homogeneous reductions of nitrogen-containing substrates catalyzed by molybdenum(IV) complexes with μ-sulfido ligands. *Organometallics* **1986**, *5*, 951.

(7) (a) Appel, A. M.; Lee, S.-J.; Franz, J. A.; DuBois, D. L.; Rakowski DuBois, M.; Birnbaum, J. C.; Twamley, B. Formation and Reactivity of a Persistent Radical in a Dinuclear Molybdenum Complex. *J. Am. Chem. Soc.* **2008**, *130*, 8940. (b) Bursten, B. E.; Cayton, R. H. Electronic structure of piano-stool dimers. 8. Electronically induced conformational changes in high-valent bimetallic chalcogen complexes of the type $[CpML]_2(\mu\text{-}L)_2$ (M = molybdenum rhenium; L = S, O). *Inorg. Chem.* **1989**, *28*, 2846. (e) Bruce, A. E.; Tyler, D. R. Photochemical isomerization of $[Cp^*MoS(\mu\text{-}S)]_2$ (Cp^* = η5-$(Me)_5C_5$) to $Cp^*Mo_4(\mu\text{-}S_2)$(.mu.-S)$_2$ and $[Cp^*MoS]_2(\mu\text{-}S_2)$. *Inorg. Chem.* **1984**, *23*, 3433.

(8) Algarra, A. G. Computational Insights into the Mechanisms of H_2 Activation and H_2/D_2 Isotope Exchange by Dimolybdenum Tetrasulfide Complexes. *Eur. J. Inorg. Chem.* **2016**, *2016*, 1886.

(9) (a) Ienco, A.; Calhorda, M. J.; Reinhold, J.; Reineri, F.; Bianchini, C.; Peruzzini, M.; Vizza, F.; Mealli, C. Activation of Molecular Hydrogen over a Binuclear Complex with Rh_2S_2 Core: DFT Calculations and NMR Mechanistic Studies. *J. Am. Chem. Soc.* **2004**, *126*, 11954. (b) Bianchini, C.; Mealli, C.; Meli, A.; Sabat, M. Reversible double addition of hydrogen on a bis(μ-sulfido) binuclear rhodium complex. *Inorg. Chem.* **1986**, *25*, 4617.

(10) Olechnowicz, F.; Hillhouse, G. L.; Jordan, R. F. Synthesis and Reactivity of NHC-Supported $Ni_2(\mu^2\text{-}\eta^2,\eta^2\text{-}S_2)$-Bridging Disulfide and $Ni_2(\mu\text{-}S)_2$-Bridging Sulfide Complexes. *Inorg. Chem.* **2015**, *54*, 2705.

(11) Compound **2** slowly decomposes at 80 °C with a first-order rate constant of ca. 1×10^{-6} s^{-1}, to produce IPr═S and an uncharacterized paramagnetic product. This decomposition precluded kinetic analysis by observation of the growth of **2**. Compound **1** is stable at 80 °C, but decomposes slowly at 90 °C.

(12) The concentration of dissolved hydrogen in benzene is proportional to the applied pressure. See: (a) Sartori, E.; Ruzzi, M.; Turro, N. J.; Decatur, J. D.; Doetschman, D. C.; Lawler, R. G.; Buchachenko, A. L.; Murata, Y.; Komatsu, K. Nuclear Relaxation of H_2 and $H_2@C_{60}$ in Organic Solvents. *J. Am. Chem. Soc.* **2006**, *128*, 14752. (b) Tsuji, T.; Shinya, Y.; Hiaki, T.; Itoh, N. Hydrogen solubility in a chemical hydrogen storage medium, aromatic hydrocarbon, cyclic hydrocarbon, and their mixture for fuel cell systems. *Fluid Phase Equilib.* **2005**, *228*−*229*, 499. (c) Park, J.; Robinson, R. L.; Gasem, K. A. M. Solubilities of Hydrogen in Aromatic Hydrocarbons from 323 to 433 K and Pressures to 21.7 MPa. *J. Chem. Eng. Data* **1996**, *41*, 70. (d) Brainard, A. J.; Williams, B. Vapor-liquid equilibrium for the system hydrogen—benzene—cyclohexane—n-hexane. *AIChE J.* **1967**, *13*, 60.

(13) Zimmer-De Iuliis, M.; Morris, R. H. Kinetic Hydrogen/Deuterium Effects in the Direct Hydrogenation of Ketones Catalyzed by a Well-Defined Ruthenium Diphosphine Diamine Complex. *J. Am. Chem. Soc.* **2009**, *131*, 11263.

(14) Bernskoetter, W. H.; Lobkovsky, E.; Chirik, P. J. Kinetics and Mechanism of N_2 Hydrogenation in Bis(cyclopentadienyl) Zirconium Complexes and Dinitrogen Functionalization by 1,2-Addition of a Saturated C−H Bond. *J. Am. Chem. Soc.* **2005**, *127*, 14051.

(15) (a) Esteruelas, M. A.; Olivan, M.; Vélez, A. POP−Rhodium-Promoted C−H and B−H Bond Activation and C−B Bond Formation. *Organometallics* **2015**, *34*, 1911. (b) Buil, M. L.; Cardo, J. J. F.; Esteruelas, M. A.; Fernández, I.; Oñate, E. Hydroboration and Hydrogenation of an Osmium−Carbon Triple Bond: Osmium Chemistry of a Bis-σ-Borane. *Organometallics* **2015**, *34*, 547. (c) Esteruelas, M. A.; Fernández, I.; López, A. M.; Mora, M.; Oñate, E. Osmium-Promoted Dehydrogenation of Amine−Boranes and B−H Bond Activation of the Resulting Amino−Boranes. *Organometallics* **2014**, *33*, 1104. (d) Buil, M. L.; Esteruelas, M. A.; Fernández, I.; Izquierdo, S.; Oñate, E. Cationic Dihydride Boryl and Dihydride Silyl Osmium(IV) NHC Complexes: A Marked Diagonal Relationship. *Organometallics* **2013**, *32*, 2744. (e) Nagaraja, C. M.; Parameswaran, P.; Jemmis, E. D.; Jagirdar, B. R. Heterolytic Activation of H−X (X = H, Si, B, and C) Bonds: An Experimental and Theoretical Investigation. *J. Am. Chem. Soc.* **2007**, *129*, 5587.

(16) (a) Jones, R. A.; Norman, N. C.; Seeberger, M. H.; Atwood, J. L.; Hunter, W. E. Synthesis and x-ray crystal structure of $[M(\mu\text{-}(Me_3C)(H)P)(PMe_3)_2]_2$ (M = Rh, Ni) containing rhodium:rhodium double and nickel-nickel single bonds. *Organometallics* **1983**, *2*, 1629. (b) Jones, R. A.; Whittlesey, B. R. Synthesis and structures of dinuclear nickel(I) di-tert-butylarsenido complexes: x-ray crystal structures of $[Ni(\mu\text{-tert-}Bu_2As)(PMe_3)]_2$ (Ni-Ni) and $[Ni(\mu\text{-tert-}Bu_2As)(CN\text{-p-tol})_2]_2$ (Ni-Ni) (tol = tolyl). *Inorg. Chem.* **1986**, *25*, 852. (c) Morgenstern, D. A.; Ferrence, G. M.; Washington, J.; Henderson, J. I.; Rosenhein, L.; Heise, J. D.; Fanwick, P. E.; Kubiak, C. P. A Class of Halide-Supported Trinuclear Nickel Clusters $[Ni_3(\mu_3\text{-}L)(\mu_3\text{-}X)(\mu_2\text{-dppm})_3]^{n+}$ (L = I^-, Br^-, CO, CNR; X = I^-, Br^-; n = 0, 1; dppm = $Ph_2PCH_2PPh_2$): Novel Physical Properties and the Fermi Resonance of Symmetric $\mu_3\text{-}\eta^1$ Bound Isocyanide Ligands. *J. Am. Chem. Soc.* **1996**, *118*, 2198. (d) Kriley, C. E.; Woolley, C. J.; Krepps, M. K.; Popa, E. M.; Fanwick, P. E.; Rothwell, I. P. Synthesis and characterization of a series of novel nickel(II)/nickel(I) complexes. Crystal structures of $[NiCl_2(dcpm)]$, $[Ni(dcpm)_2](NO_3)_2\cdot 2EtOH$, $[Ni_2Cl_2(\mu\text{-dcpm})_2(\mu\text{-H})]$ and $[Ni_2(\mu\text{-}PCy_2)_2(PCy_2Me)_2]$; dcpm = bis(dicyclohexylphosphino)methane. *Inorg. Chim. Acta* **2000**, *300*−*302*, 200. (e) Ito, M.; Matsumoto, T.; Tatsumi, K. Synthesis and Reactions of Mono- and Dinuclear Ni(I) Thiolate Complexes. *Inorg. Chem.* **2009**, *48*, 2215. (f) Inosako, A.; Kunishita, A.; Kubo, M.; Ogura, T.; Sugimoto, H.; Itoh, S. ($\mu\text{-}\eta^2\text{:}\eta^2$-Disulfido)dinickel(II) complexes supported by 6-methyl-TPA ligands. *Dalton Trans.* **2009**, 9410.

DOI: 10.1021/acs.inorgchem.7b01420
Inorg. Chem. 2017, 56, 9922−9930

(g) Varonka, M. S.; Warren, T. H. Three-Coordinate N-Heterocyclic Carbene Nickel Nitrosyl Complexes. *Organometallics* **2010**, *29*, 717.

(17) A CSD search performed on 6/1/2017 found 202 3-coordinate B-S complexes, with B−S bond lengths spanning of 1.720−1.895 Å and an average of 1.82 Å.

(18) (a) Cámpora, J.; Cartes, M. Á.; Rodríguez-Delgado, A.; Naz, A. M.; Palma, P.; Pérez, C. M.; del Rio, D. Studies on the Atropisomerism of Fe(II) 2,6-Bis(*N*-arylimino)pyridine Complexes. *Inorg. Chem.* **2009**, *48*, 3679. (b) Rodríguez-Delgado, A.; Cámpora, J.; Naz, A. M.; Palma, P.; Reyes, M. L. Separation of a diiminopyridine iron(II) complex into *rac*- and *meso*- diastereoisomers provides evidence for a dual stereoregulation mechanism in propene polymerization. *Chem. Commun.* **2008**, 5230.

(19) Oster, S. S.; Jones, W. D. Structural properties and inversion mechanisms of $[Rh(dippe)(\mu\text{-SR})]_2$ complexes. *Inorg. Chim. Acta* **2004**, *357*, 1836.

(20) Dekker, M.; Knox, G. R.; Robertson, C. G. Hydrocarbon metal sulphide complexes IV. Some observations on the isomerisation of bis-μ-(arylthio)bis(carbonylcyclopentadienyliron). *J. Organomet. Chem.* **1969**, *18*, 161.

(21) (a) Chauhan, R.; Mashuta, M. S.; Grapperhaus, C. A. Selective and Reversible Base-Induced Elimination of a Ruthenium Dithioether Yields a Vinyl Metallosulfonium Complex. *Inorg. Chem.* **2012**, *51*, 7913. (b) Adams, H.; Amado, A. M.; Félix, V.; Mann, B. E.; Antelo-Martinez, J.; Newell, M.; Ribeiro-Claro, P. J. A.; Spey, S. E.; Thomas, J. A. Ru^{II} Complexes Incorporating Tetrathiamacrocycles: Synthesis and Conformational Analysis. *Chem. - Eur. J.* **2005**, *11*, 2031. (c) Baradello, L.; Lo Schiavo, S.; Nicolò, F.; Lanza, S.; Alibrandi, G.; Tresoldi, G. Restricted Phenyl Rotation in Pyridyl Thioether Ligands N,S-Chelated to Congested Diiminoruthenium Cores. *Eur. J. Inorg. Chem.* **2004**, *2004*, 3358. (d) Tresoldi, G.; Lo Schiavo, S.; Lanza, S.; Cardiano, P. A Congested $Ru(dps)_2$ or $Ru(dprs)_2$ Core (dps = di-2-pyridyl sulfide; dprs = di-2-pyrimidinyl sulfide) Promotes Sulfur Inversion of *N,S*-Chelate Thioethers Containing CH_2R and 2-Pyridyl or 2-Pyrimidinyl Groups. *Eur. J. Inorg. Chem.* **2002**, *2002*, 181. (e) Abel, E. W.; Ahmed, A. K. S.; Farrow, G. W.; Orrell, J. G.; Sik, V. Nuclear magnetic resonance study of inversion at sulphur and selenium atoms in complexes of palladium(II) and platinum(II). Part 2. Complexes of methyl and phenyl trimethylsilylmethyl sulphide and selenide. *J. Chem. Soc., Dalton Trans.* **1977**, 47. (f) Rauk, A.; Allen, L. C.; Mislow, K. Pyramidal Inversion. *Angew. Chem., Int. Ed. Engl.* **1970**, *9*, 400.

(22) (a) Kalläne, S. I.; Braun, T.; Teltewskoi, M.; Braun, B.; Herrmann, R.; Laubenstein, R. Remarkable reactivity of a rhodium(I) boryl complex towards CO_2 and CS_2: isolation of a carbido complex. *Chem. Commun.* **2015**, *51*, 14613. (b) Ahrens, T.; Schmiedecke, B.; Braun, T.; Herrmann, R.; Laubenstein, R. Activation of CS_2 and COS at a Rhodium(I) Germyl Complex: Generation of CS and Carbido Complexes. *Eur. J. Inorg. Chem.* **2017**, *2017*, 713.

(23) Esteruelas, M. A.; López, A. M.; Mora, M.; Oñate, E. B−H activation and H−H formation: two consecutive heterolytic processes on an osmium−hydrogensulfide bond. *Chem. Commun.* **2013**, *49*, 7543.

(24) For other routes to borylthiolate compounds, see: (a) Romero, E. A.; Peltier, J. L.; Jazzar, R.; Bertrand, G. Catalyst-free dehydrocoupling of amines, alcohols, and thiols with pinacol borane and 9-borabicyclononane (9-BBN). *Chem. Commun.* **2016**, *52*, 10563. (b) Yang, Z.; Zhong, M.; Ma, X.; Nijesh, K.; De, S.; Parameswaran, P.; Roesky, H. W. An Aluminum Dihydride Working as a Catalyst in Hydroboration and Dehydrocoupling. *J. Am. Chem. Soc.* **2016**, *138*, 2548. (c) Fernandez-Salas, J. A.; Manzini, S.; Nolan, S. P. Efficient ruthenium-catalysed S−S, S−Si and S−B bond forming reactions. *Chem. Commun.* **2013**, *49*, 5829. (d) Carter, C. A. G.; Vogels, C. M.; Harrison, D. J.; Gagnon, M. K. J.; Norman, D. W.; Langler, R. F.; Baker, R. T.; Westcott, S. A. Metal-Catalyzed Hydroboration and Diboration of Thiocarbonyls and Vinyl Sulfides. *Organometallics* **2001**, *20*, 2130. (e) Siebert, W.; Gast, E.; Riegel, F.; Schmidt, M. Thio- und selenoborsäuren. *J. Organomet. Chem.* **1975**, *90*, 13.

(25) For synthetic applications of borylthiolate compounds, see: (a) Civit, M. G.; Royes, J.; Vogels, C. M.; Westcott, S. A.; Cuenca, A. B.; Fernández, E. Strategic Trimethylsilyldiazomethane Insertion into pinB−SR Followed by Selective Alkylations. *Org. Lett.* **2016**, *18*, 3830. (b) Ishiyama, T.; Mori, M.; Suzuki, A.; Miyaura, N. The palladium-catalyzed cross-coupling reaction of 9-organothio-9-borabicyclo[3.3.1]nonanes with organic electrophiles: Synthesis of unsymmetrical sulfides. *J. Organomet. Chem.* **1996**, *525*, 225. (c) Ishiyama, T.; Nishijima, K.; Miyaura, N.; Suzuki, A. Palladium-(0)-catalyzed thioboration of terminal alkynes with 9-(alkylthio)-9-borabicyclo[3.3.1]nonane derivatives: stereoselective synthesis of vinyl sulfides via the thioboration-cross-coupling sequence. *J. Am. Chem. Soc.* **1993**, *115*, 7219.

(26) A CSD search performed on 6/1/2017 did not find any 3-coordinate $S\text{-}BO_2$ units that bridge two metal centers.

(27) (a) Wübbolt, S.; Maji, M. S.; Irran, E.; Oestreich, M. A Tethered Ru−S Complex with an Axial Chiral Thiolate Ligand for Cooperative Si−H Bond Activation: Application to Enantioselective Imine Reduction. *Chem. - Eur. J.* **2017**, *23*, 6213. (b) Bähr, S.; Simonneau, A.; Irran, E.; Oestreich, M. An Air-Stable Dimeric Ru−S Complex with an NHC as Ancillary Ligand for Cooperative Si−H Bond Activation. *Organometallics* **2016**, *35*, 925. (c) Milstein, D. Metal−ligand cooperation by aromatization−dearomatization as a tool in single bond activation. *Philos. Trans. R. Soc., A* **2015**, *373*, 20140189. (d) Khusnutdinova, J. R.; Milstein, D. Metal−Ligand Cooperation. *Angew. Chem., Int. Ed.* **2015**, *54*, 12236. (e) Stevenson, L.; Mellino, S.; Clot, E.; Mountford, P. Reactions of Titanium Hydrazides with Silanes and Boranes: N−N Bond Cleavage and N Atom Functionalization. *J. Am. Chem. Soc.* **2015**, *137*, 10140. (f) Stahl, T.; Hrobarik, P.; Konigs, C. D.; Ohki, Y.; Tatsumi, K.; Kemper, S.; Kaupp, M.; Klare, H. F. T.; Oestreich, M. Mechanism of the cooperative Si−H bond activation at Ru−S bonds. *Chem. Sci.* **2015**, *6*, 4324. (g) Stahl, T.; Muther, K.; Ohki, Y.; Tatsumi, K.; Oestreich, M. Catalytic Generation of Borenium Ions by Cooperative B−H Bond Activation: The Elusive Direct Electrophilic Borylation of Nitrogen Heterocycles with Pinacolborane. *J. Am. Chem. Soc.* **2013**, *135*, 10978. (h) Klare, H. F. T.; Oestreich, M.; Ito, J.-i.; Nishiyama, H.; Ohki, Y.; Tatsumi, K. Cooperative Catalytic Activation of Si−H Bonds by a Polar Ru−S Bond: Regioselective Low-Temperature C−H Silylation of Indoles under Neutral Conditions by a Friedel−Crafts Mechanism. *J. Am. Chem. Soc.* **2011**, *133*, 3312. (i) Ikariya, T. Chemistry of *Concerto* Molecular Catalysis Based on the Metal/NH Bifunctionality. *Bull. Chem. Soc. Jpn.* **2011**, *84*, 1. (j) Seino, H.; Misumi, Y.; Hojo, Y.; Mizobe, Y. Heterolytic H_2 activation by rhodium thiolato complexes bearing the hydrotris-(pyrazolyl)borato ligand and application to catalytic hydrogenation under mild conditions. *Dalton Trans.* **2010**, *39*, 3072. (k) Misumi, Y.; Seino, H.; Mizobe, Y. Heterolytic Cleavage of Hydrogen Molecule by Rhodium Thiolate Complexes That Catalyze Chemoselective Hydrogenation of Imines under Ambient Conditions. *J. Am. Chem. Soc.* **2009**, *131*, 14636. (l) Ohki, Y.; Sakamoto, M.; Tatsumi, K. Reversible Heterolysis of H_2 Mediated by an M−S(Thiolate) Bond (M = Ir, Rh): A Mechanistic Implication for [NiFe] Hydrogenase. *J. Am. Chem. Soc.* **2008**, *130*, 11610. (m) Sellmann, D.; Prakash, R.; Heinemann, F. W.; Moll, M.; Klimowicz, M. Heterolytic Cleavage of H_2 at a Sulfur-Bridged Dinuclear Ruthenium Center. *Angew. Chem., Int. Ed.* **2004**, *43*, 1877. (n) Sweeney, Z. K.; Polse, J. L.; Bergman, R. G.; Andersen, R. A. Dihydrogen Activation by Titanium Sulfide Complexes. *Organometallics* **1999**, *18*, 5502. (o) Sellmann, D.; Rackelmann, G. H.; Heinemann, F. W. Heterolytic Activation of Dihydrogen at Transition-Metal Sulfur Sites in Coordinatively Unsaturated $[Rh(L)(\text{“}^{bu}S_4\text{”})]BF_4$ Complexes, Involving Neutral Hydrides, Thiol Hydrides, and Thiol−Hydride Proton Scrambling (L = CO, PCy_3; $\text{“}^{bu}S_4\text{”}^{2-}$ = 1,2-Bis[(2-mercapto-3,5-di-*tert*-butylphenylthio]ethane^{2-}). *Chem. - Eur. J.* **1997**, *3*, 2071.

(28) Pangborn, A. B.; Giardello, M. A.; Grubbs, R. H.; Rosen, R. K.; Timmers, F. J. Safe and Convenient Procedure for Solvent Purification. *Organometallics* **1996**, *15*, 1518.

(29) Sheldrick, G. M. Crystal structure refinement with *SHELXL*. *Acta Crystallogr., Sect. C: Struct. Chem.* **2015**, *C71*, 3.

DOI: 10.1021/acs.inorgchem.7b01420
Inorg. Chem. 2017, 56, 9922−9930

(30) Dolomanov, O. V.; Bourhis, L. J.; Gildea, R. J.; Howard, J. A. K.; Puschmann, H. *OLEX2*: a complete structure solution, refinement and analysis program. *J. Appl. Crystallogr.* **2009**, *42*, 339.
(31) Sheldrick, G. M. A short history of *SHELX*. *Acta Crystallogr., Sect. A: Found. Crystallogr.* **2008**, *A64*, 112.
(32) Frisch, M. J.; Trucks, G. W.; Schlegel, H. B.; et al. *Gaussian 09*, Revision, D.01; Gaussian, Inc.: Wallingford, CT, 2009.
(33) Svensson, M.; Humbel, S.; Froese, R. D.; Matsubara, T.; Sieber, S.; Morokuma, K. ONIOM: A Multilayered Integrated MO + MM Method for Geometry Optimizations and Single Point Energy Predictions. A Test for Diels–Alder Reactions and $Pt(P(t\text{-}Bu)_3)_2$ + H_2 Oxidative Addition. *J. Phys. Chem.* **1996**, *100*, 19357.
(34) Rassolov, V. A.; Ratner, M. A.; Pople, J. A.; Redfern, P. C.; Curtiss, L. A. 6-31G* basis set for third-row atoms. *J. Comput. Chem.* **2001**, *22*, 976.

DOI: 10.1021/acs.inorgchem.7b01420
Inorg. Chem. 2017, 56, 9922–9930